

Electronic Supplementary Material (ESI) for Journal of Materials Chemistry A.  
This journal is © The Royal Society of Chemistry 2018

## Supplementary Information

# Understanding on the structural and electrochemical performance of orthorhombic sodium manganese oxides

Ji Ung Choi<sup>a</sup>, Chong Seung Yoon<sup>b</sup>, Qian Zhang<sup>c</sup>, Payam Kaghazchi<sup>c</sup>, Young Hwa Jung<sup>d</sup>, Kug-Seung Lee<sup>d</sup>, Do-Cheon Ahn<sup>d</sup>, Yang-Kook Sun<sup>e,\*</sup> and Seung-Taek Myung<sup>a,\*</sup>

<sup>a</sup>Department of Nano Technology and Advanced Materials Engineering, Sejong University, Seoul 05006, South Korea

<sup>b</sup>Department of Materials Science and Engineering, Hanyang University, Seoul, 04763, Republic of Korea

<sup>c</sup>Institut für Chemie und Biochemie, Freie Universität Berlin, Takustr. 3, Berlin 14195, Germany

<sup>d</sup>Beamline Department, Pohang Accelerator Laboratory (PAL), Pohang 37673, South Korea

<sup>e</sup>Department of Energy Engineering, Hanyang University, Seoul 04763, South Korea

---

\* Corresponding author

E-mail: smyung@sejong.ac.kr (S. Myung), yksun@hanyang.ac.kr (Y. Sun)

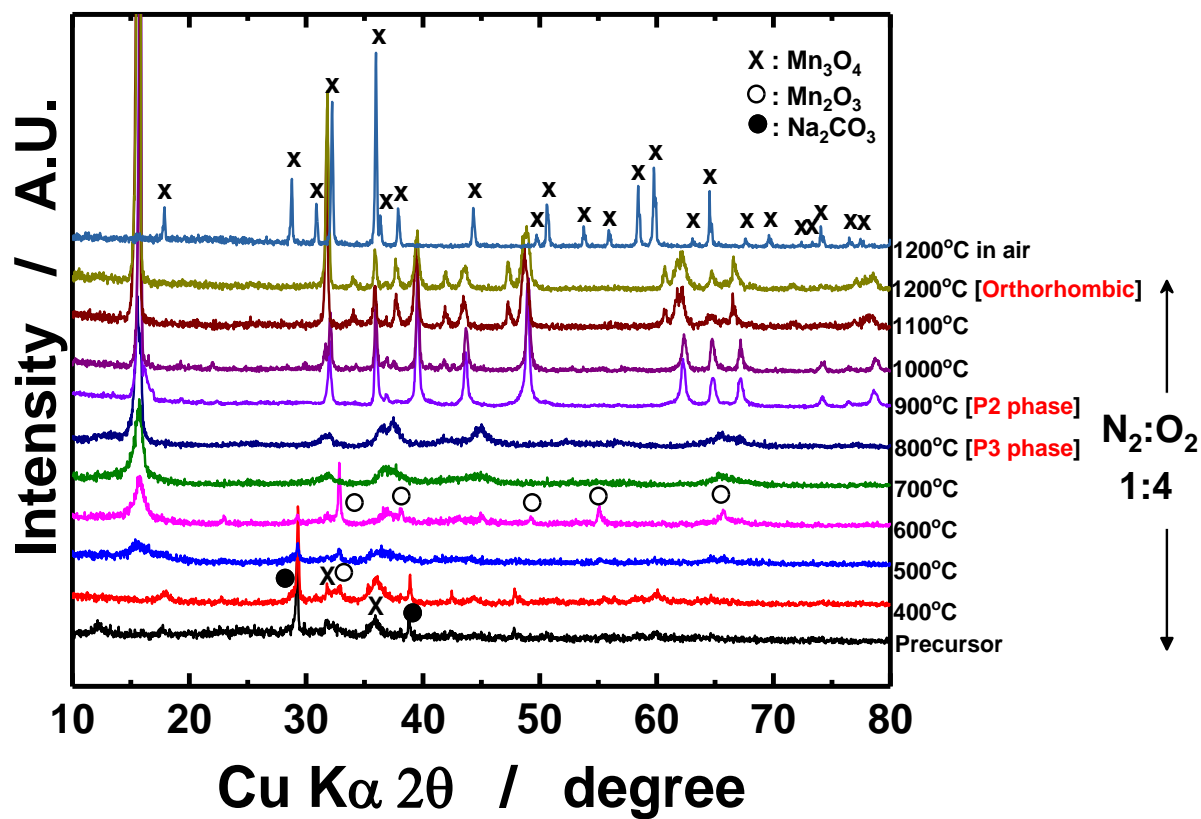
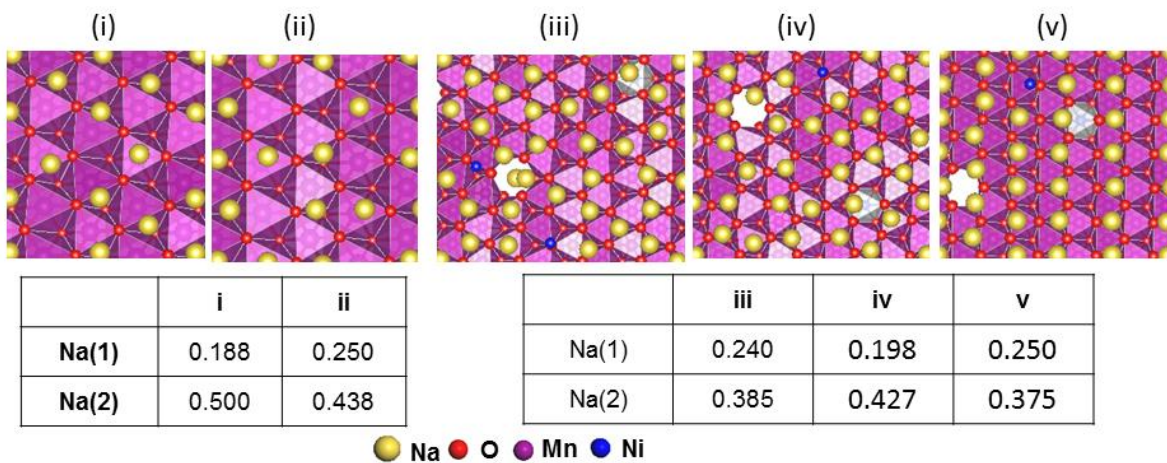
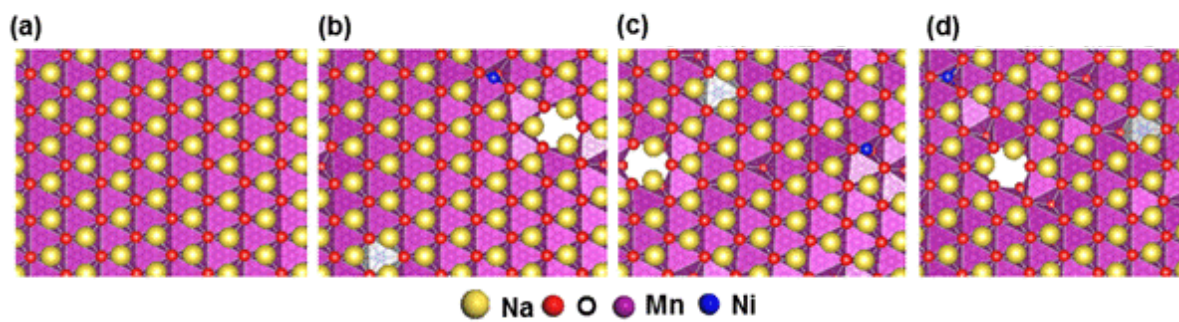


Figure SI-1. XRD patterns of the compounds obtained on increasing the calcination temperature.



**Figure SI-2.** Top views and occupancies of Na sites for *o*-Na<sub>0.68</sub>MnO<sub>2</sub> (configurations i and ii) and *o*-[Na<sub>0.625</sub>Ni<sub>0.02</sub>][Mn<sub>0.96</sub>Ni<sub>0.02</sub>]O<sub>2</sub> (configurations iii, iv, and v).



**Figure SI-3.** Top views of (a)  $o$ -NaMnO<sub>2</sub>, (b)  $o$ -[Na<sub>0.96</sub>Ni<sub>0.02</sub>][Mn<sub>0.96</sub>Ni<sub>0.02</sub>]O<sub>2</sub>, (c)  $o$ -[Na<sub>0.90</sub>Ni<sub>0.02</sub>][Mn<sub>0.96</sub>Ni<sub>0.02</sub>]O<sub>2</sub>, and (d)  $o$ -[Na<sub>0.85</sub>Ni<sub>0.02</sub>][Mn<sub>0.96</sub>Ni<sub>0.02</sub>]O<sub>2</sub>.

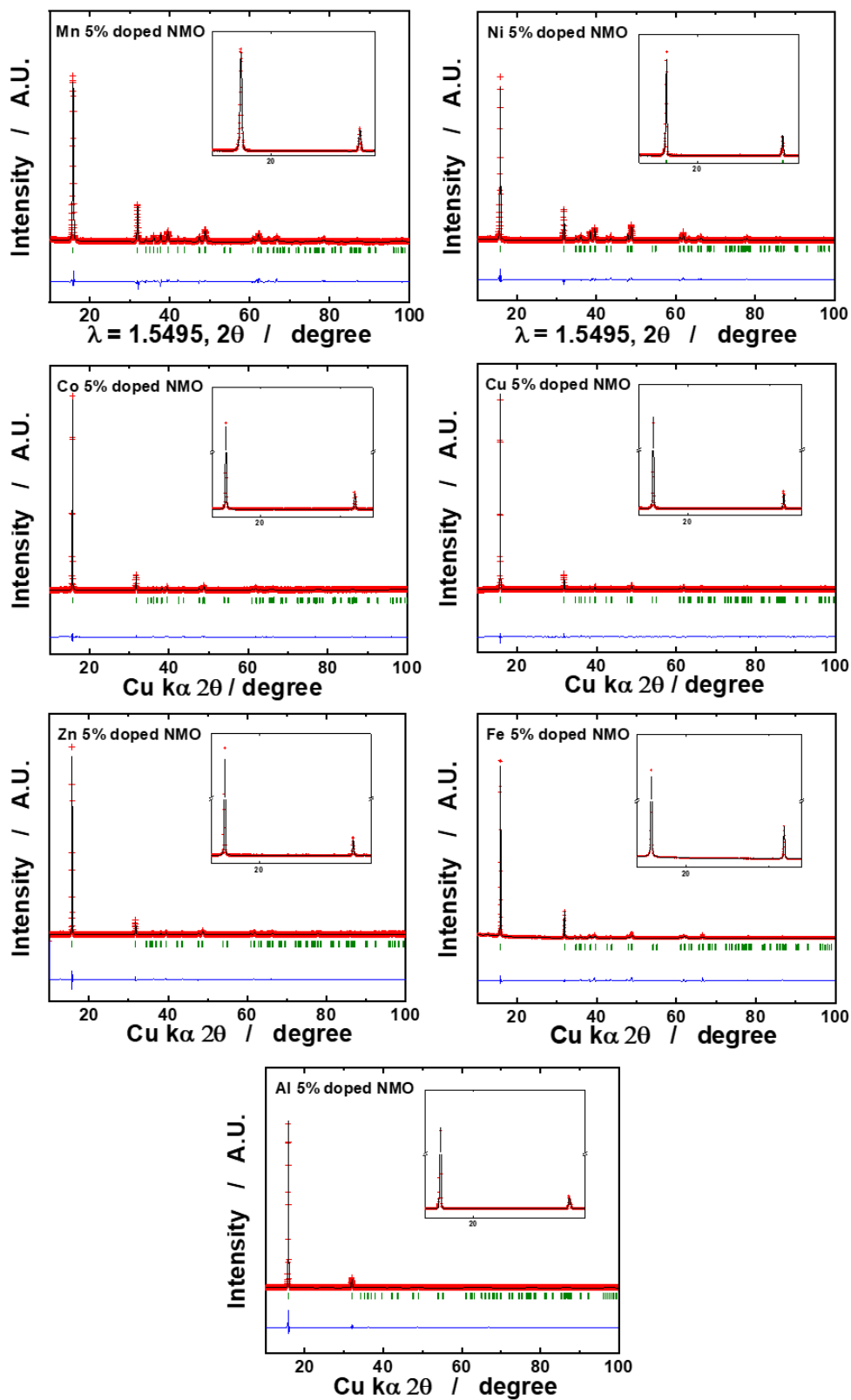


**Figure SI-4.** Rietveld refinement patterns of synchrotron and power XRD patterns for  $o$ - $\text{Na}_{0.67}[\text{M}_{0.05}\text{Mn}_{0.95}]\text{O}_2$  materials ( $\text{M} = \text{Mn}, \text{Ni}, \text{Co}, \text{Cu}, \text{Zn}, \text{Fe},$  and  $\text{Al}$ ). An enlargement is also shown in the inset corresponding to the  $(002)_{\text{P}2}$  and  $(004)_{\text{P}2}$  reflection.

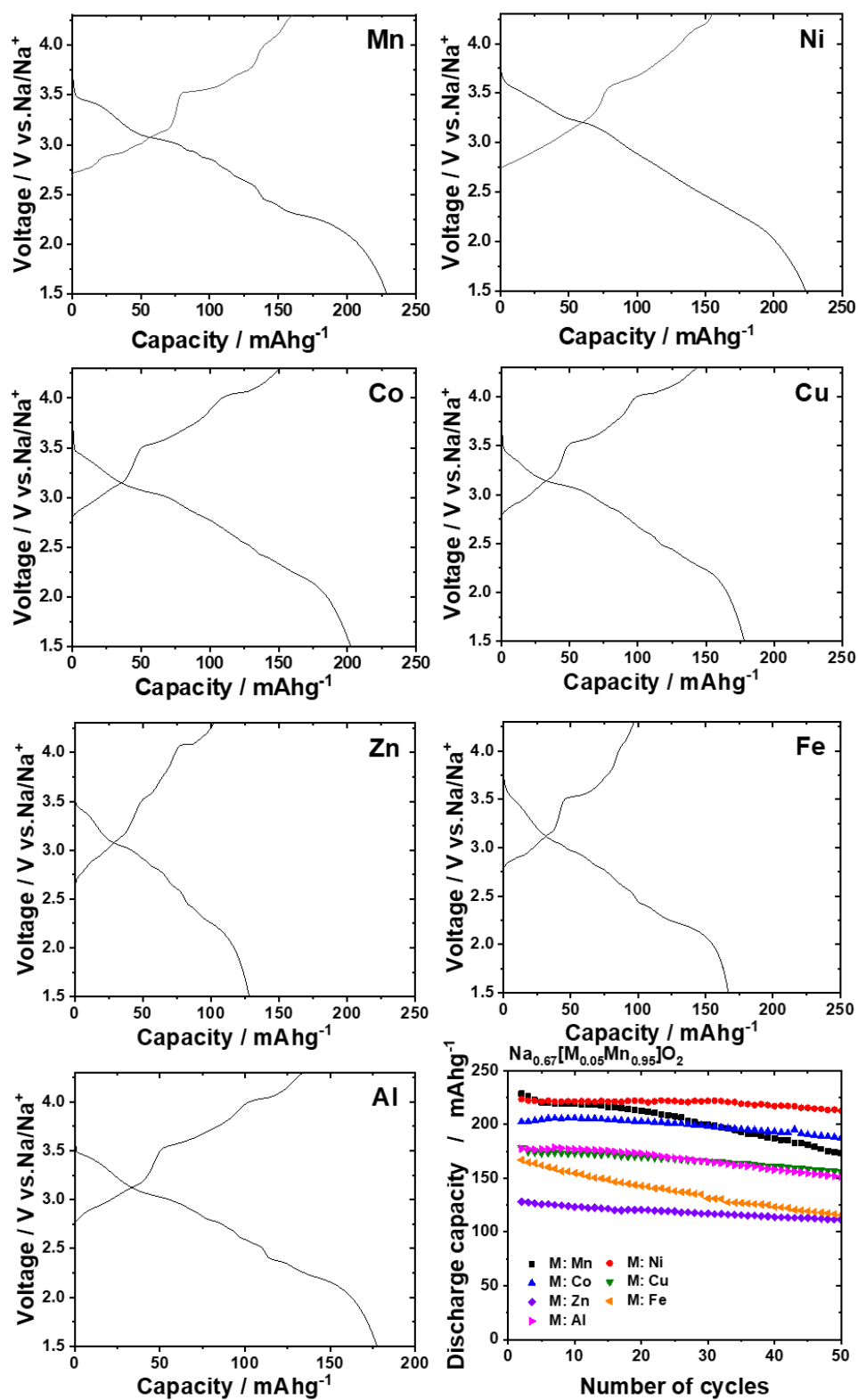


**Figure SI-5.** The voltage profiles and cycling performance of  $o\text{-Na}_{0.67}[\text{M}_{0.05}\text{Mn}_{0.95}]\text{O}_2$  (M = Mn, Ni, Co, Cu, Zn, Fe and Al).

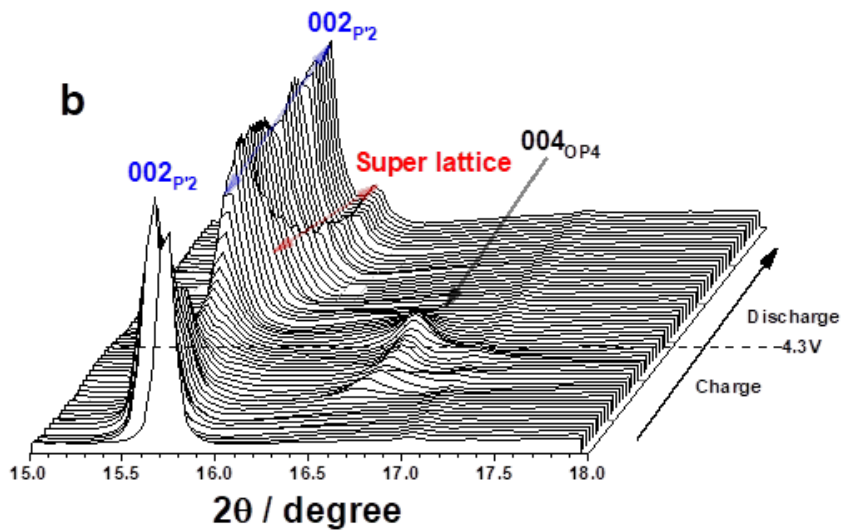
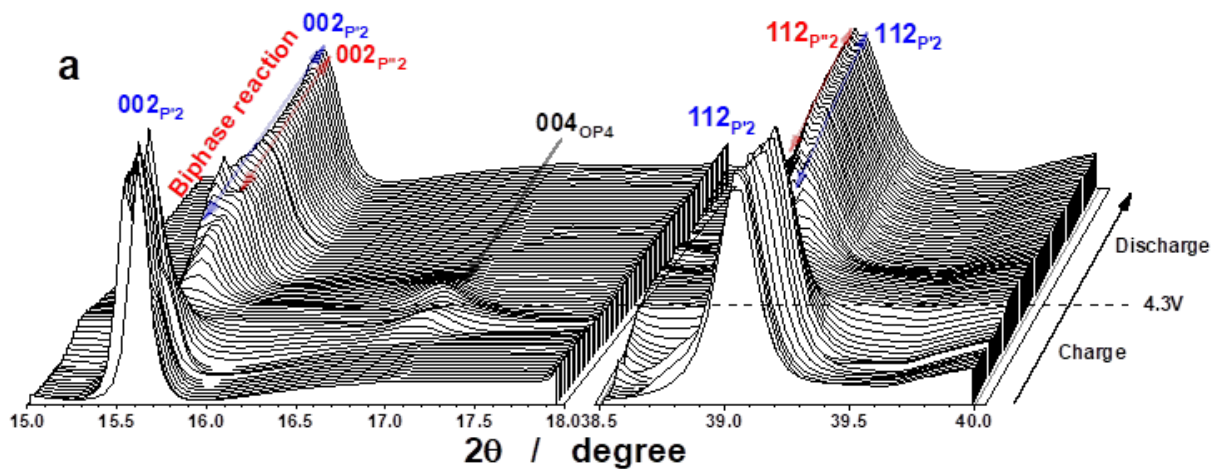


**Figure SI-6.** Magnified *in situ* synchrotron XRD patterns for (a)  $o\text{-Na}_{0.67}\text{MnO}_2$  and (b)  $o\text{-Na}_{0.67}[\text{Ni}_{0.05}\text{Mn}_{0.95}]\text{O}_2$  electrodes recorded during one cycle in Figure 3.

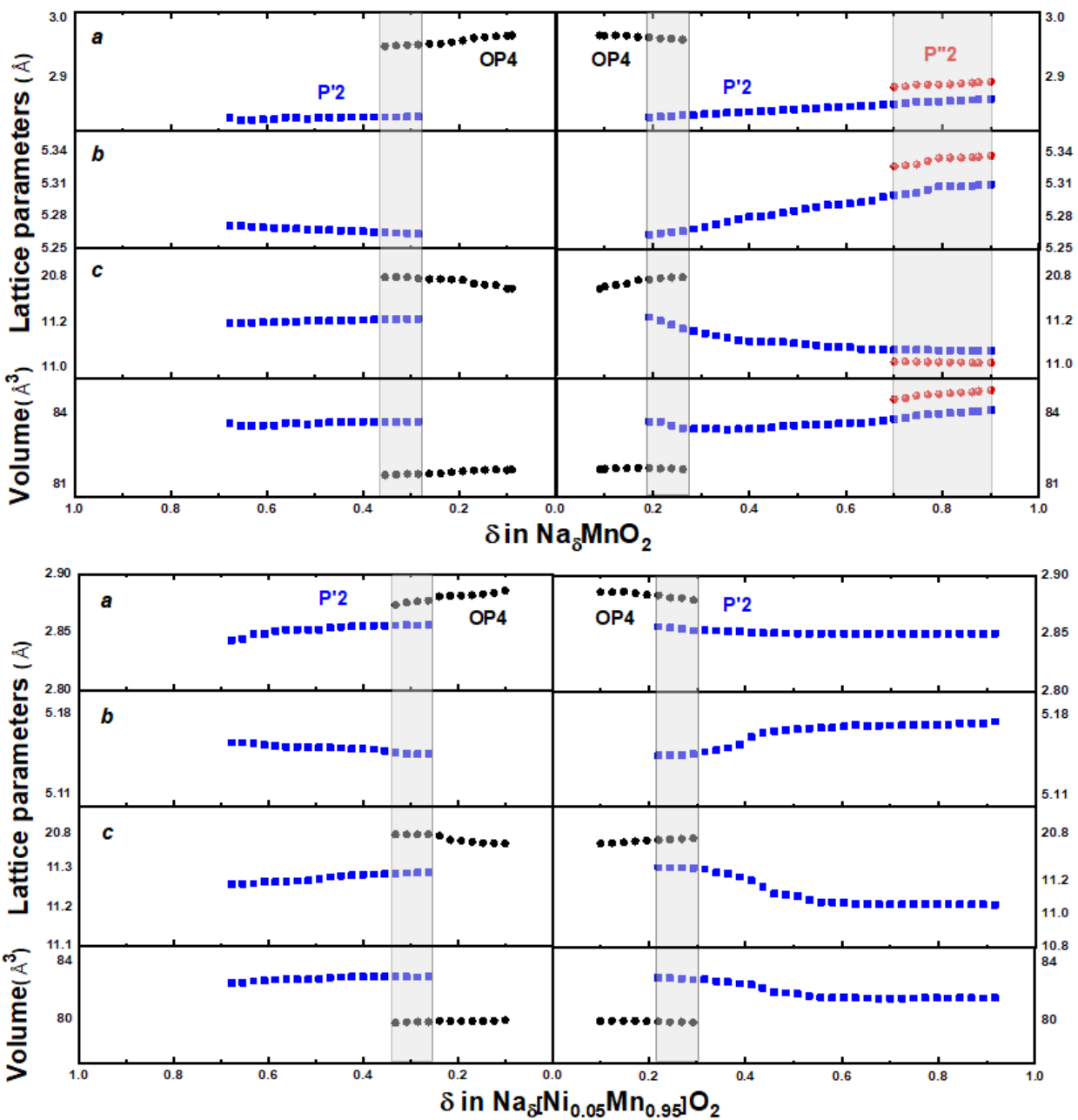


**Figure SI-7.** Evolution of the  $a$ ,  $b$ , and  $c$  cell parameters and the lattice volume of P'2, P''2 and OP4 phases during one cycle calculated from *in situ* S-XRD for a)  $o\text{-Na}_{0.67}\text{MnO}_2$  and b)  $o\text{-Na}_{0.67}[\text{Ni}_{0.05}\text{Mn}_{0.95}]\text{O}_2$ .



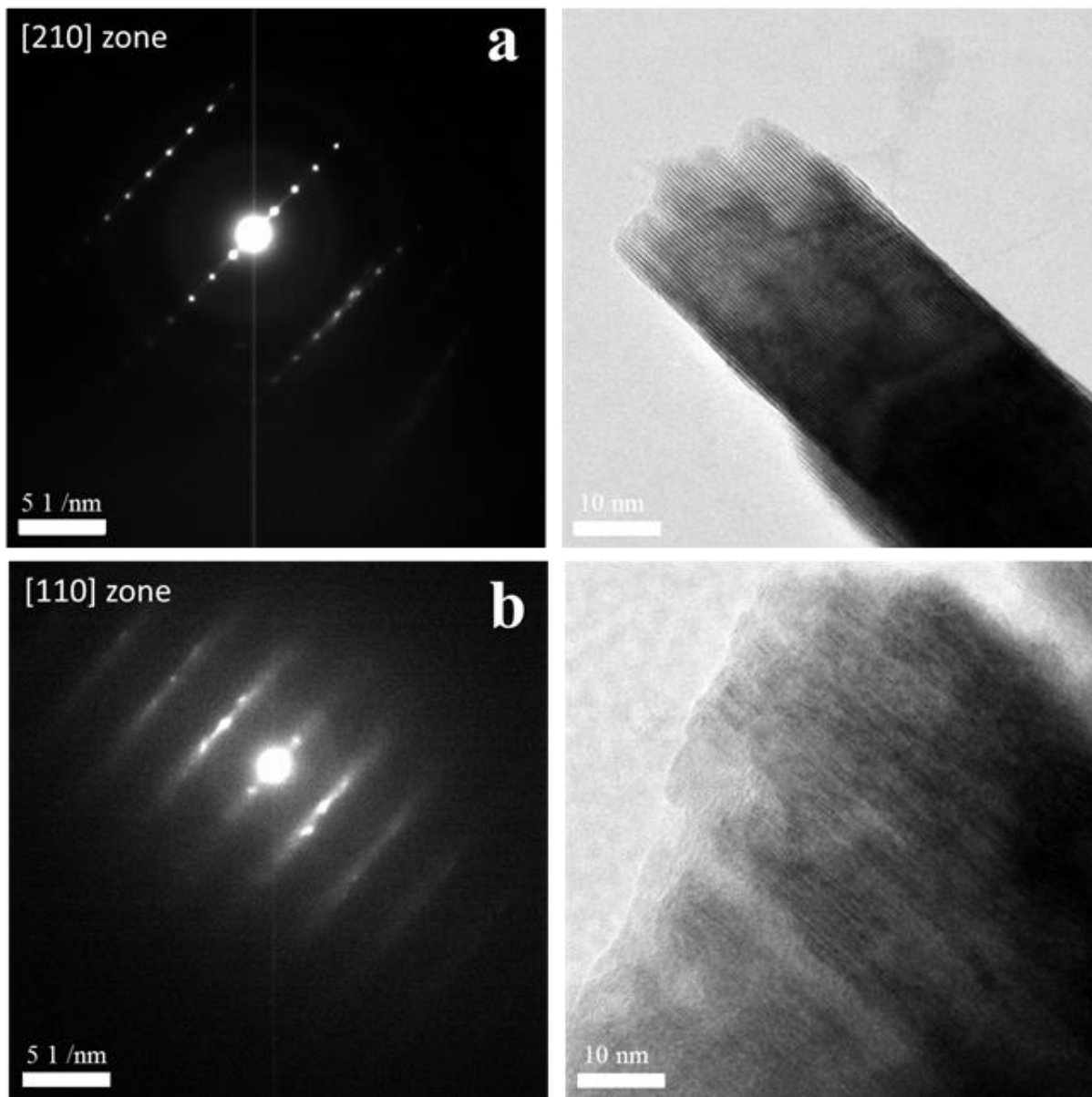


**Figure SI-8.** (a) The [210] zone diffraction pattern and high-resolution image of  $o\text{-Na}_{0.67}\text{MnO}_2$  after 1<sup>st</sup> cycle and (b) [110] zone diffraction pattern and high-resolution image of  $o\text{-Na}_{0.67}[\text{Ni}_{0.05}\text{Mn}_{0.95}]\text{O}_2$  after the 50<sup>th</sup> cycle.

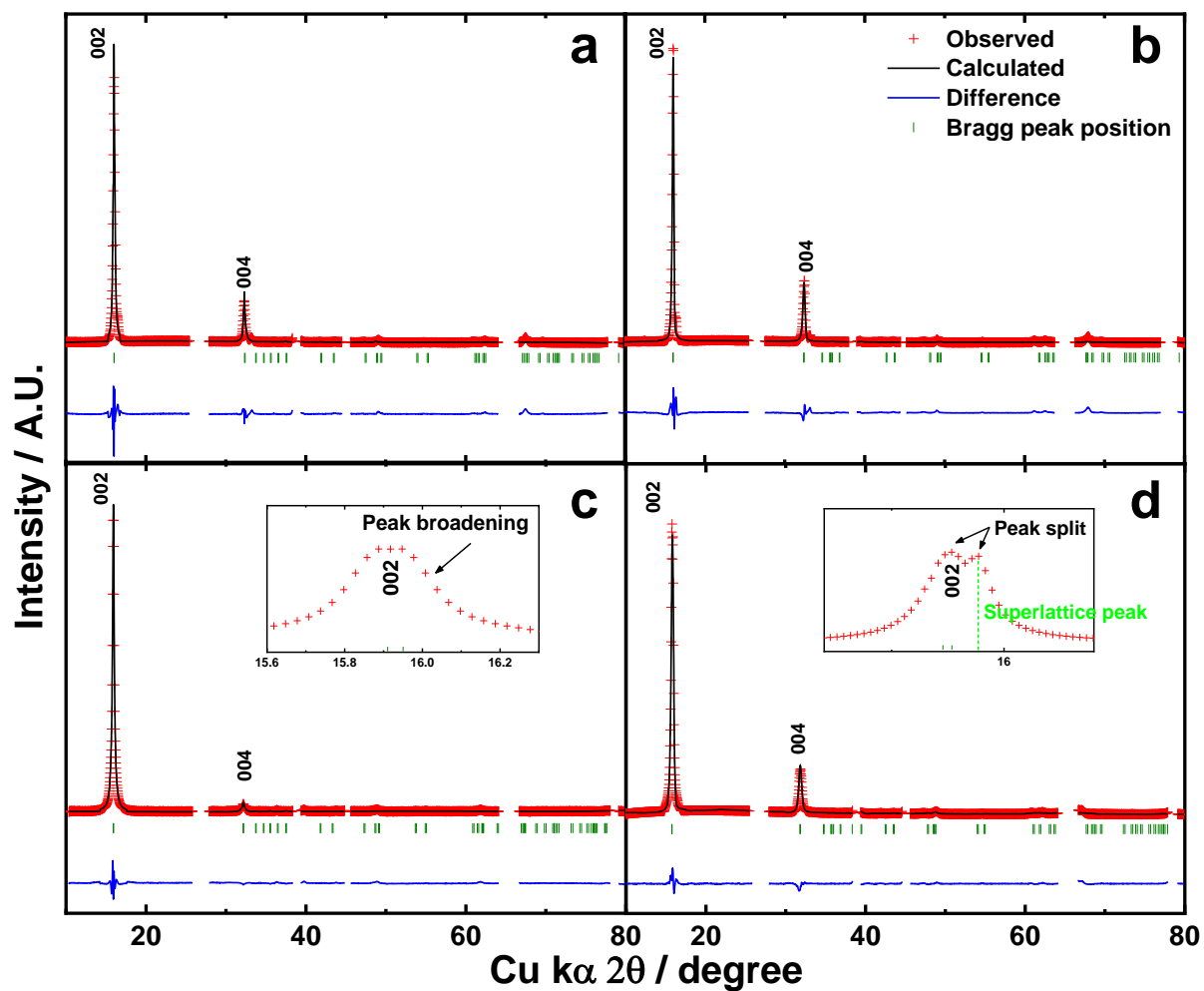


**Figure SI-9.** Rietveld Refinement of the *ex situ* XRD patterns for (a,c)  $o\text{-Na}_{0.67}\text{MnO}_2$  (b,d)  $o\text{-Na}_{0.67}[\text{Ni}_{0.05}\text{Mn}_{0.95}]\text{O}_2$  electrodes after one and extensive cycling, respectively. An enlargement is also shown in the inset corresponding to the  $(002)_{P_2}$  reflection.

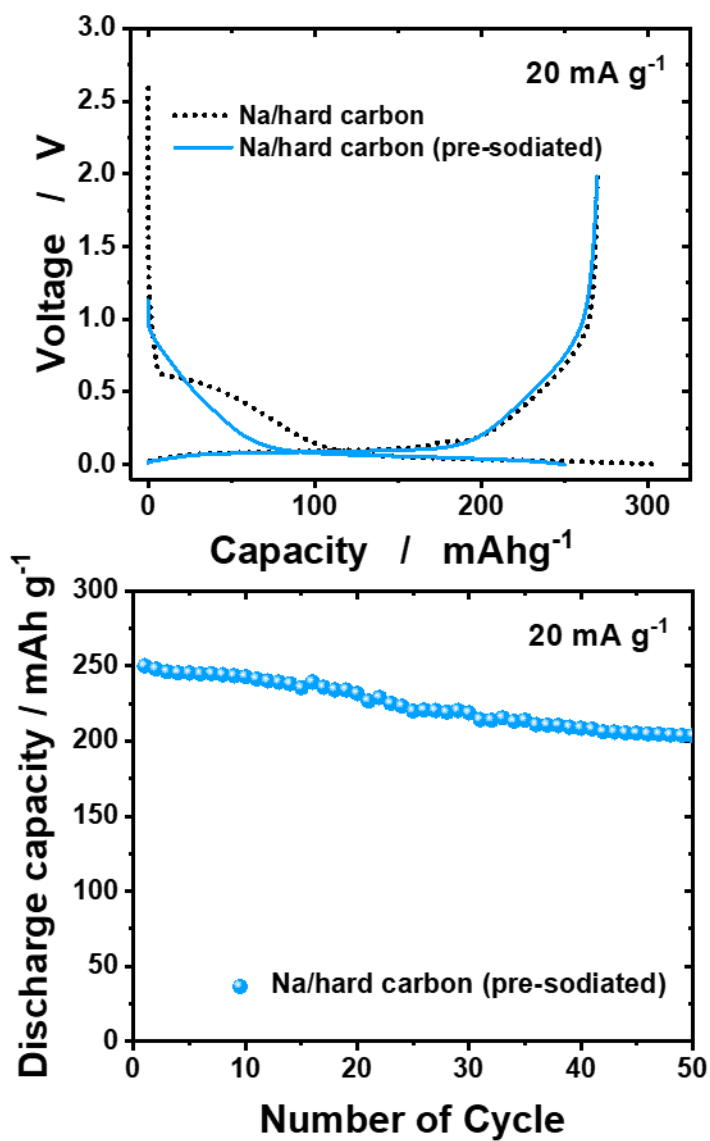


**Figure SI-10.** Hard carbon (a) First discharge-charge curves of Na/hard carbon and Na/hard carbon (pre-sodiated) and (b) Cyclability of sodium cell for 50 cycles of Na/hard carbon (pre-sodiated).

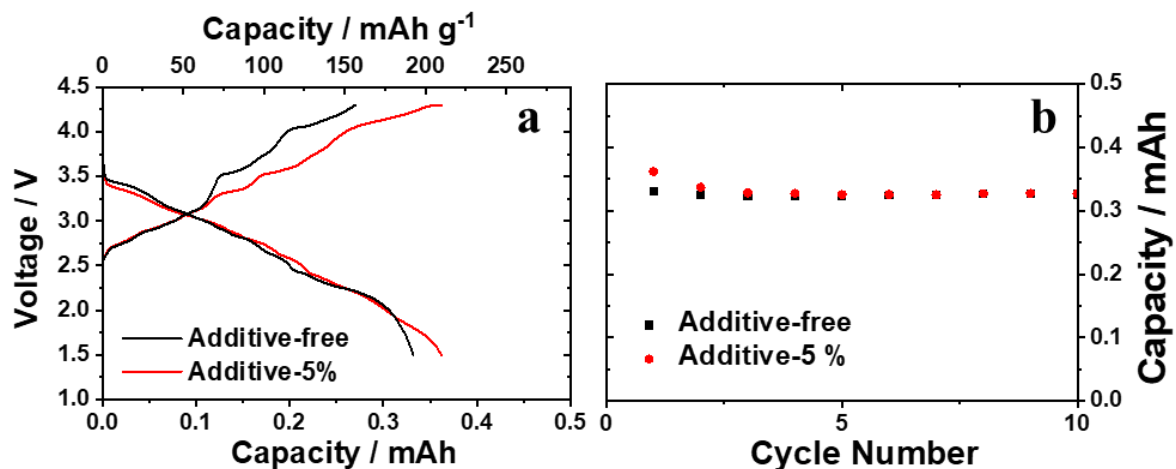


**Figure SI-11.** Comparison of (a) the first charge-discharge capacities and (b) cycling performance for 10 cycles assisted by the sacrificing salt additive tested in *o*-Na<sub>0.67</sub>[Co<sub>0.05</sub>Mn<sub>0.95</sub>]O<sub>2</sub> with a weight ratio of 95:5 (active material:NaNO<sub>2</sub> additive).

During electrochemical desodiation, the NaNO<sub>2</sub> was oxidatively decomposed by the following reaction: NaNO<sub>2</sub> → NO<sub>2</sub> + Na<sup>+</sup> + e<sup>-</sup>. As anticipated, the initial charge capacity was able to increase which was similar to the initial discharge capacity with 100% Coulombic efficiency (Figure SI-11a) with acceptable electrode performances (Figures SI-11b).

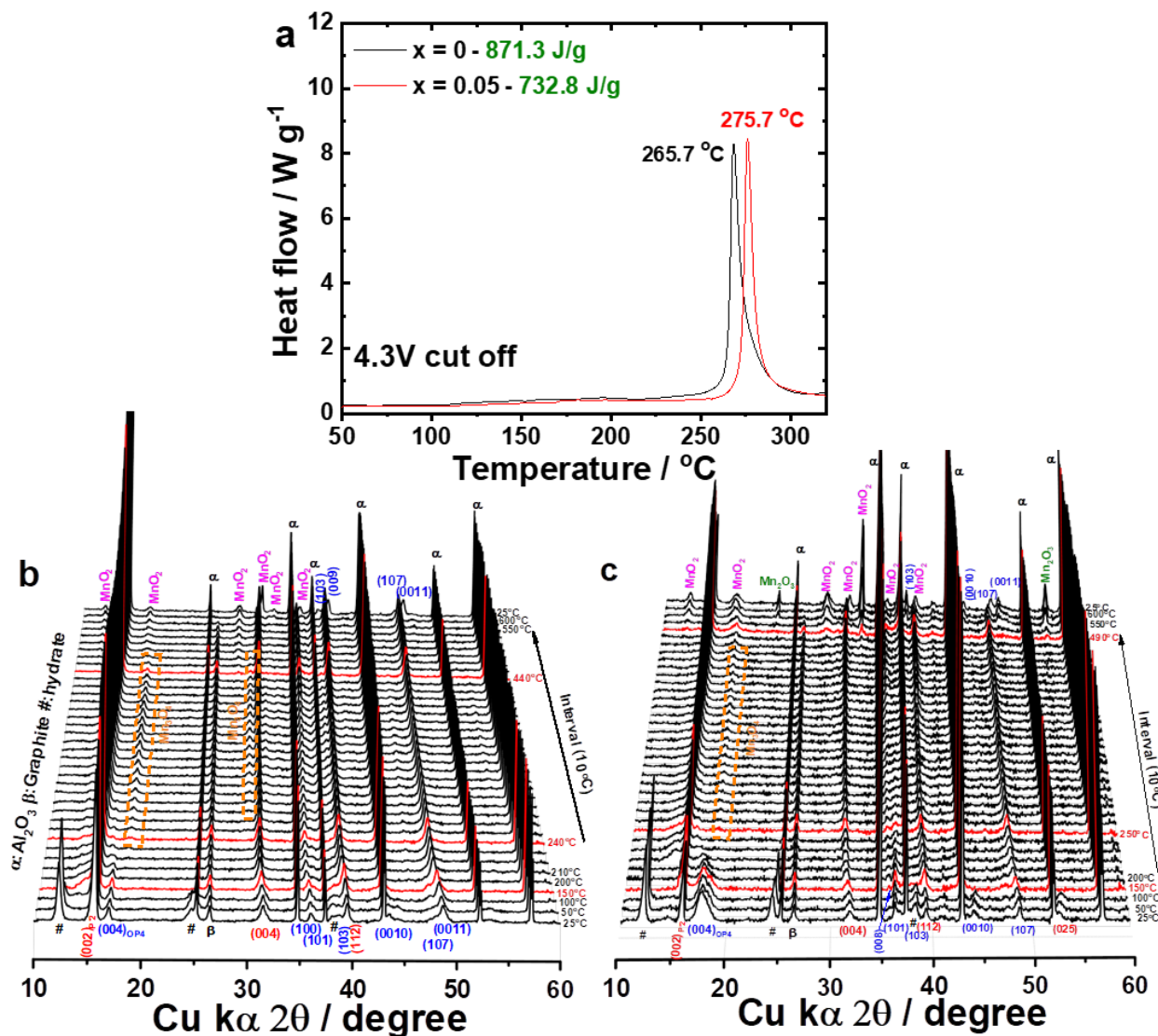


**Figure SI-12.** (a) Differential scanning calorimetry curves of desodiated  $o\text{-Na}_{0.05}[\text{Ni}_x\text{Mn}_{1-x}]\text{O}_2$  ( $x = 0$  and 0.05) obtained after charging to 4.3 V and *in situ* high-temperature XRD patterns of electrochemically desodiated (b)  $o\text{-Na}_{0.05}\text{MnO}_2$  and (c)  $o\text{-Na}_{0.05}[\text{Ni}_{0.05}\text{Mn}_{0.95}]\text{O}_2$ .

The heat evolution of the exothermic processes was measured for desodiated  $o\text{-Na}_{0.05}[\text{Ni}_x\text{Mn}_{1-x}]\text{O}_2$  ( $x = 0$  and 0.05) (Figure SI-12a). As anticipated, both desodiated compounds exhibited main exothermic reactions in the temperature range of 260–300 °C. Because the exothermic reaction is mainly related to the evaporation of oxygen from the crystal structure, the oxygen evolution triggers the partial formation of spinel  $\text{Mn}_3\text{O}_4$ , which is obvious for both samples in this temperature range. In particular, Ni-doped  $o\text{-Na}_{0.05}[\text{Ni}_{0.05}\text{Mn}_{0.95}]\text{O}_2$  induced a slight shift of the main exothermic reaction toward higher temperatures with reduced heat generation because of the lower amount of oxygen evolution, as confirmed by the TGA data (Figure SI-13). This suggests that Ni doping in the Mn-matrix is effective in delaying oxygen

evolution, although the P'2 and OP4 structures are dominant in the high-temperature XRD patterns (Figures SI-12b and c). Further heating caused the formation of MnO<sub>2</sub> above 420 °C for *o*-Na<sub>0.05</sub>MnO<sub>2</sub> and 450 °C for the Ni-doped *o*-Na<sub>0.05</sub>[Ni<sub>0.05</sub>Mn<sub>0.95</sub>]O<sub>2</sub>. After cooling, the P'2 and OP4 structures were still evident as major phases in the XRD patterns, emphasizing the structural stability of these Mn-based materials. In summary, the effect of Ni doping into P'2 *o*-Na<sub>0.67</sub>[Ni<sub>*x*</sub>Mn<sub>1-*x*</sub>]O<sub>2</sub> affects not only its superior electrochemical performance but also improves its thermal stability in the highly desodiated state.

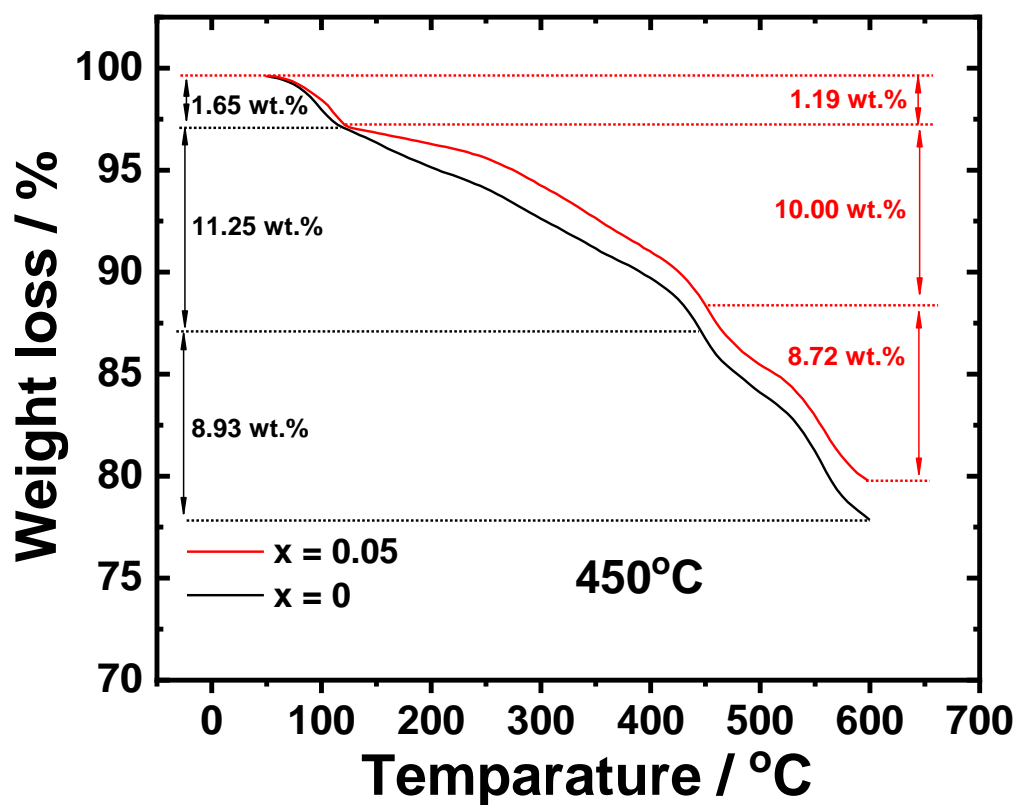


**Figure SI-13.** Thermogravimetric analysis curves of chemically desodiated  $o\text{-Na}_{0.05}[\text{Ni}_x\text{Mn}_{1-x}]\text{O}_2$  ( $x = 0$  and 0.05, respectively) obtained after charging to 4.3 V.

**Table SI-1.** Rietveld refinement results of S-XRD data for  $o$ - $\text{Na}_{0.67}\text{MnO}_2$  and  $o$ - $\text{Na}_{0.67}[\text{Ni}_{0.05}\text{Mn}_{0.95}]\text{O}_2$  calcined at 1200 °C for 10 h in a dry air atmosphere and the resulting electric conductivity.

$\text{Na}_{0.67}\text{MnO}_2$		<b>x</b>	<b>y</b>	<b>z</b>	<b>g</b>	<b><math>B/\text{Å}</math></b>
Na <sub>f</sub> (1)	4c	0	-0.0668	0.25	0.214	3.154
Na <sub>e</sub> (2)	4c	0	0.3189	0.25	0.456	1.383
Mn	4a	0	0	0	1.0	0.27
O	8f	0	0.6504	0.0975	1.0	0.73
$R_{\text{wp}}$						12.6 %
$\text{Na}_{0.67}[\text{Ni}_{0.05}\text{Mn}_{0.95}]\text{O}_2$		<b>x</b>	<b>y</b>	<b>z</b>	<b>g</b>	<b><math>B/\text{Å}</math></b>
Na <sub>f</sub> (1)	4c	0	-0.0680	0.25	0.237	3.5
Ni	4c	0	-0.0680	0.25	0.011	3.5
Na <sub>e</sub> (2)	4c	0	0.3	0.25	0.399	2.6
Ni	4c	0	0.3	0.25	0.014	2.6
Mn	4a	0	0	0	0.975	0.42
Ni	4a	0	0	0	0.025	0.42
O	8f	0	0.6666	0.0934	1.0	0.85
$R_{\text{wp}}$						13.7 %



**Table SI-2.** Summary of refined crystallographic parameters, degree of distortion and electric conductivity for  $o\text{-Na}_{0.67}[\text{M}_{0.05}\text{Mn}_{0.95}]\text{O}_2$  materials (M = Mn, Ni, Co, Cu, Zn, Fe, and Al).

<b>Lattice parameters</b>							
$\text{Na}_{0.67}[\text{M}_{0.05}\text{Mn}_{0.95}]\text{O}_2$							
<b>Electrodes</b>	<i>a</i> -axis/Å	<i>b</i> -axis/Å	<i>c</i> -axis/Å	$R_{\text{wp}}/\%$	<b>Degree of distortion / %</b>	<b>Electric conductivity /S cm<sup>-1</sup></b>	
M = Mn	2.8314(0)	5.2715(3)	11.1968(6)	12.6	7.0	$6.8 \times 10^{-6}$	
M = Ni	2.8434(1)	5.1551(1)	11.2664(8)	13.7	4.5	$5.2 \times 10^{-5}$	
M = Co	2.8387(2)	5.1830(6)	11.2750(5)	11.3	5.1	$1.3 \times 10^{-5}$	
M = Cu	2.8383(4)	5.1835(7)	11.2714(8)	12.3	5.2	$1.1 \times 10^{-6}$	
M = Zn	2.8445(4)	5.1832(8)	11.2714(1)	13.2	4.9	$5.1 \times 10^{-6}$	
M = Fe	2.8400(8)	5.1656(3)	11.2280(6)	12.7	4.7	$8.9 \times 10^{-6}$	
M = Al	2.8338(9)	5.2340(3)	11.1763(2)	12.2	6.2	$6.7 \times 10^{-6}$	

**Table SI-3.** Calculated lattice parameters of bulk *o*-NaMnO<sub>2</sub> using different U-J values for Mn.

<b>U-J [eV]</b>	<b><i>a</i> [Å]</b>	<b><i>b</i> [Å]</b>	<b><i>c</i> [Å]</b>
3.0	2.90	5.74	10.81
4.0	2.92	5.73	10.85

**Table SI-4.** Calculated lattice constants for bare and Ni-doped *o*-Na<sub>x</sub>MnO<sub>2</sub> models. Ni dopants (5%) are located at both Na and Mn sites. Experimental values are also given for comparison.

Lattice parameters	<i>a</i> -axis/Å		<i>b</i> -axis/Å		<i>c</i> -axis/Å	
	Exp	Theo	Exp	Theo	Exp	Theo
Na <sub>0.67</sub> MnO <sub>2</sub>	2.83	2.88	5.27	5.42	11.20	11.12
[Na <sub>0.62</sub> Ni <sub>0.02</sub> ][Mn <sub>0.96</sub> Ni <sub>0.02</sub> ]O <sub>2</sub>	2.84	2.94	5.16	5.22	11.27	11.17
NaMnO <sub>2</sub> *	2.86	2.90	5.31	5.73	11.06	10.81
[Na <sub>0.96</sub> Ni <sub>0.02</sub> ][Mn <sub>0.96</sub> Ni <sub>0.02</sub> ]O <sub>2</sub> *	2.85	2.90	5.17	5.63	11.05	10.77
Na <sub>0.92</sub> MnO <sub>2</sub>	-	2.90	-	5.64	-	10.85
[Na <sub>0.90</sub> Ni <sub>0.02</sub> ][Mn <sub>0.96</sub> Ni <sub>0.02</sub> ]O <sub>2</sub>	-	2.90	-	5.58	-	10.81
[Na <sub>0.85</sub> Ni <sub>0.02</sub> ][Mn <sub>0.96</sub> Ni <sub>0.02</sub> ]O <sub>2</sub>	-	2.90	-	5.51	-	10.83

\*The values were obtained from electrochemical sodiation (after 1st discharge to 1.5 V). Details are shown in Table S5.

**Table SI-5.** Lattice parameter from Rietveld refinement after one cycle.

<b>After one cycled</b> $\text{Na}_{0.67}[\text{M}_{0.05}\text{Mn}_{0.95}]\text{O}_2$	<b>Lattice parameters</b>		
	<i>a</i> -axis/Å	<i>b</i> -axis/Å	<i>c</i> -axis/Å
M = Mn	2.8644(7)	5.3102(0)	11.0625(8)
M = Ni	2.8579(1)	5.1738(5)	11.0580(9)

**Table SI-6.** Lattice parameter from Rietveld refinement after extensive cycles.

After extensive cycled		<i>x</i>	<i>y</i>	<i>z</i>	<i>g</i>	B/Å
<b>Na<sub>0.67</sub>MnO<sub>2</sub></b>						
Na <sub>f</sub> (1)	4c	0	-0.0668	0.25	0.435	3.154
Na <sub>e</sub> (2)	4c	0	0.31894	0.25	0.558	1.383
Mn	4a	0	0	0	1.0	0.27
O	8f	0	0.87731	0.09874	1.0	0.73
Space group: <i>Cmcm</i> , <i>a</i> = 2.8728(2) Å, <i>b</i> = 5.3156(1) Å, <i>c</i> = 11.1312(8) Å						
<i>Rwp</i> /% = 13.3%						
After extensive cycled		<i>x</i>	<i>y</i>	<i>z</i>	<i>g</i>	B/Å
<b>Na<sub>0.67</sub>[Ni<sub>0.05</sub>Mn<sub>0.95</sub>]O<sub>2</sub></b>						
Na <sub>f</sub> (1)	4c	0	-0.0680	0.25	0.363	3.5
Ni	4c	0	-0.0680	0.25	0.011	3.5
Na <sub>e</sub> (2)	4c	0	0.3	0.25	0.587	2.6
Ni	4c	0	0.3	0.25	0.014	2.6
Mn	4a	0	0	0	0.975	0.42
Ni	4a	0	0	0	0.025	0.42
O	8f	0	0.6666	0.09340	1.0	0.85
Space group: <i>Cmcm</i> , <i>a</i> = 2.8551(5) Å, <i>b</i> = 5.1630(4) Å, <i>c</i> = 11.2594(1) Å						
<i>Rwp</i> /% = 8.19%						